Effect of Ge doping on growth stress and conductivity in Al_xGa_{1-x}N •

Cite as: Appl. Phys. Lett. 114, 142101 (2019); https://doi.org/10.1063/1.5080680 Submitted: 10 November 2018. Accepted: 20 March 2019. Published Online: 08 April 2019

Anushka Bansal, Ke Wang, James Spencer Lundh, Sukwon Choi, and Joan M. Redwing 🔟



COLLECTIONS



This paper was selected as Featured







ARTICLES YOU MAY BE INTERESTED IN

Anisotropic phonon properties and effective electron mass in a-Ga₂O₃ Applied Physics Letters 114, 142102 (2019); https://doi.org/10.1063/1.5086731

Graphene-assisted quasi-van der Waals epitaxy of AIN film for ultraviolet light emitting diodes on nano-patterned sapphire substrate

Applied Physics Letters 114, 091107 (2019); https://doi.org/10.1063/1.5081112

A critical review of recent progress on negative capacitance field-effect transistors Applied Physics Letters 114, 090401 (2019); https://doi.org/10.1063/1.5092684





Effect of Ge doping on growth stress and conductivity in Al_xGa_{1-x}N ⁽¹⁾

Cite as: Appl. Phys. Lett. **114**, 142101 (2019); doi: 10.1063/1.5080680 Submitted: 10 November 2018 · Accepted: 20 March 2019 · Published Online: 8 April 2019







Anushka Bansal, Ke Wang, James Spencer Lundh, Sukwon Choi, and Joan M. Redwing la

AFFILIATIONS

- Department of Materials Science and Engineering, The Pennsylvania State University, University Park, Pennsylvania 16802, USA
- ²Materials Characterization Laboratory, Materials Research Institute, The Pennsylvania State University, University Park, Pennsylvania 16802, USA
- Department of Mechanical Engineering, The Pennsylvania State University, University Park, Pennsylvania 16802, USA

ABSTRACT

Silicon (Si) is a common n-type donor in $Al_xGa_{1-x}N$; however, it induces bending of edge-type threading dislocations which can generate tensile stress in the film leading to the formation of channeling cracks in thick layers. Germanium (Ge) has previously been investigated as an alternative to Si for n-type doping of GaN, but its impact on film stress in $Al_xGa_{1-x}N$ has not been investigated in detail. In this study, we employ in situ wafer curvature measurements combined with postgrowth characterization to investigate Ge doping of $Al_xGa_{1-x}N$ (x=0–0.62) layers grown on 6H-SiC by metalorganic chemical vapor deposition. It was found that Ge doping ($n\sim 1.6-10^{19}$ cm⁻³) of $Al_{0.30}Ga_{0.70}N$ does not induce tensile stress during growth in contrast to that observed with a similar level of Si doping. In addition, the average inclination angle of edge dislocations was similar for undoped and Ge doped films indicating that Ge does not promote surface-mediated dislocation climb. High n-type doping was achieved in Ge doped $Al_xGa_{1-x}N$ for lower Al fraction range (x<0.5), but resistivity increased and carrier density decreased significantly for higher Al fractions. The results demonstrate Ge doping as a viable alternative to Si doping of $Al_xGa_{1-x}N$ (x<0.5) for achieving thick, crack-free layers.

Published under license by AIP Publishing. https://doi.org/10.1063/1.5080680

Intentional n-type doping of $Al_xGa_{1-x}N$ has been widely studied both experimentally and theoretically given its critical role in current group III-nitride light-emitting diodes (LEDs) and high electron mobility transistors (HEMTs) as well as emerging applications in ultrawide bandgap devices. ^{1–5} Silicon, the most intensively investigated donor impurity, is an effective n-type dopant in $Al_xGa_{1-x}N^{1,2,6}$ for Al fractions up to \sim 80%–90% after which a sharp decrease in carrier density and a steep increase in donor activation energy have been reported. ⁶ The incorporation of Si during growth of $Al_xGa_{1-x}N$ on sapphire and SiC substrates introduces tensile stress in the film with the increasing layer thickness. ^{7–10} The tensile stress is relaxed via the formation of channeling cracks that are problematic for device fabrication.

The mechanism by which Si incorporation induces tensile stress in $Al_xGa_{1-x}N$ has been discussed in prior studies. Cantu *et al.* initially observed an increase in surface roughness due to Si doping. This observation was correlated with the inclination of threading dislocations (TDs) giving rise to a misfit dislocation component indicating that Si doping promoted the relaxation of compressively strained $Al_xGa_{1-x}N$ layers. Studies by Romanov *et al.* demonstrated that these inclined edge dislocations could be

frozen-in resulting in a strain gradient that relaxes compressive stress and, after a certain thickness, generates tensile stress responsible for film cracking. 12,13 An "effective climb" mechanism was proposed whereby dislocation climb does not occur in the bulk of the material but rather is associated with diffusion and incorporation of adatoms on the growing surface. Building on this work, Follstaedt et al. proposed a "surface-mediated climb" process whereby bending is initiated and maintained by vacancies in the growing surface layer that become attached to threading dislocation cores. 14 Along similar lines, Raghavan et al. described this as a kinetic process arising from out-diffusion of atoms from dislocation cores on the growth surface. 15 Several mechanisms have been proposed to explain the influence of Si on dislocation inclination. Dadgar et al. explained it as a result of a chemical effect due to SiN_x formation at the dislocation core acting as a mask.¹⁶ However, in other work by Xie et al., this was attributed to dislocation climb via Ga vacancies on the surface that depend on the Fermi level position suggesting an electronic effect.² Nevertheless, the propensity for cracks to form in heavily Si doped Al_xGa_{1-x}N is problematic for a variety of device applications.

a) Author to whom correspondence should be addressed: jmr31@psu.edu.

As a result of the problems associated with Si-doping, Ge has been investigated as an alternative *n*-type dopant for GaN and has generally been reported to enable higher electron concentrations than Si, up to 2 10²⁰ cm ³ as reported by Fritze *et al.*¹⁷ However, conflicting results have been reported as to the effect of Ge doping on film stress. Xie *et al.* investigated Ge doping of GaN grown on (0001) sapphire using GeH₄. They reported tensile strain within the Ge doped layer as measured using high resolution X-ray diffraction (HRXRD) and also dislocation inclination as assessed by cross-sectional scanning transmission electron microscopy (STEM), beginning at the point where Ge was introduced during the growth. ¹⁸ In contrast, Fritze *et al.* reported that Ge doping of GaN grown on (0001) sapphire substrates off-oriented 0.25 towards the m-direction using GeH₄ and isobutylgermane as dopant sources did not add additional tensile stress in the film as measured by *in situ* curvature measurements along with *ex situ* HRXRD measurements.

Based on the results reported for GaN, Ge would appear to be an attractive n-type dopant for $Al_xGa_{1-x}N$. Theoretical studies predicted a decrease in carrier density and conductivity for Al fractions higher than 52% due to the formation of DX centers. Recent experimental studies by Blasco $\it et al.$ for heavily Ge doped $Al_xGa_{1-x}N$ ($\geq = 1 \quad 10^{21}$ cm 3) reported gradual decrease in the carrier concentration with increasing Al fraction up to x=0.64-0.66, at which resistivity increases significantly due to a drop in the donor activation rate. However, its impact on film stress has not yet been experimentally investigated. In the work reported here, we employed $\it in situ$ wafer curvature measurements combined with postgrowth structural characterization to investigate the effect of Ge doping on growth stress and the dislocation microstructure of the films. Hall measurements were also performed to further study the effect of the Al fraction on the resistivity and carrier density in the Ge doped $Al_xGa_{1-x}N$ films.

The Al_xGa_{1-x}N layers were grown on 1 cm 1 cm semi-insulating Si-face (0001) 6H-SiC substrates in a vertical cold wall metalorganic chemical vapor deposition (MOCVD) reactor equipped with a k-Space multibeam optical stress (MOS) sensor for in situ wafer curvature measurements. 20-22 Prior to growth, the SiC substrates were cleaned using standard solvents followed by a 10:1 HF dip to remove any native oxide. The layers were grown at a total pressure of 100 Torr, while the temperature of the susceptor was maintained at 1150 C. Initially, samples were cleaned in situ using hightemperature H₂ etch at 1150 C to ensure the removal of residual native oxide from the surface. Approximately 85 nm of aluminum nitride (AlN) was initially deposited as a buffer layer, followed by the growth of Al_xGa_{1-x}N layers (~1 μm thick). Precursor sources included trimethylaluminum (TMAl), trimethylgallium (TMGa), ultrahigh purity ammonia (NH₃) gas, silane (SiH₄; 10% in H₂), and germane (GeH₄; 2% in H₂) for Al, Ga, N, Si, and Ge sources, respectively, with hydrogen acting as a carrier gas. The AlN buffer layers were deposited at a growth rate of ~0.3 Å/s using TMAl and NH₃ flow rates of 13.8 µmol/min and 89.3 mmol/min, respectively. The Al_xGa₁ _xN films were grown at ∼3 Å/s using source flow rates of 9.2 to 4.7 μmol/min for TMGa, 2.7 to 7.2 μmol/min for TMAl, and 89.3 mmol/min for NH₃ depending on the layer composition (x = 0-0.62). Samples were prepared with an initial \sim 200 nm thick undoped Al_xGa_{1 x}N layer after which SiH₄ or GeH₄ was switched into the reactor for the remainder of the layer growth. A SiH₄/ TMGa) ratio of 2 10 3 was used for the growth of Si doped $Al_{0.30}Ga_{0.70}N$ layer $[n = 8.8 10^{18}/cm^3]$. For Ge doped

Al_{0.30}Ga_{0.70}N layers, a GeH₄/(TMAl TMGa) ratio of 0.5 was required to get a comparable doping level $[n = 1.6 10^{19}/cm^3]$. A similarly low doping efficiency with GeH₄ as compared to SiH₄ was reported for GaN in previous work by Fritze et al. 17 In fact, the gas phase dopant/metalorganic ratios that they employed for GaN growth resulted in similar carrier concentration levels as we observe for Al_{0.30}Ga_{0.70}N. The lower doping efficiency of GeH₄ is likely due to its greater gas phase reactivity compared to SiH₄. Pyrolysis studies of GeH₄ and SiH₄, for example, demonstrate that the unimolecular decomposition rate of GeH₄ is an order of magnitude higher than that of SiH₄ under similar conditions. ^{23,24} At the high growth temperatures employed for GaN and AlGaN growth, GeH4 likely undergoes substantial decomposition in the gas phase and may predeposit on reactor surfaces upstream of the substrate. Consequently, higher GeH₄ gas phase concentrations are required to achieve a similar doping level in the film as is obtained with SiH₄.

Film stress during growth and upon the introduction of dopants was measured *in situ* using the MOS sensor which measures the change in spot spacing of a linear array of reflected laser beams²⁵ from the substrate to obtain information on curvature changes. A decrease in spot spacing corresponds to a biaxial tensile stress in the film while an increase in spot spacing indicates a compressive stress. The change in spot spacing (δd) can then be converted to the product of the incremental stress (σ_f) times the film thickness (h_f) using a modified form of Stoney's equation

$$\sigma_f h_f = \left(\frac{\delta d}{d_0}\right) \frac{M_s h_s^2 \cos \theta}{12L},$$
(1)

where d_o is the initial spot spacing, M_s is the biaxial modulus of the substrate (602.2 GPa for 6H-SiC²⁶), h_s is the substrate thickness, θ is the angle of incidence of the laser beam with respect to the substrate normal, and L is the distance between the substrate and the CCD camera in the MOS sensor system. The incremental stress (σ) is equivalent to the biaxial stress in the film at the surface during growth.

Cross-sectional transmission electron microscopy (X-TEM) samples were prepared using a FEI Helios 660 focused ion beam (FIB) system. A thick protective amorphous carbon layer was deposited over the region of interest and then Ga ions (30 kV then stepped down to 1 kV to avoid ion beam damage to the sample surface) were used in the FIB to make the samples electron transparent for TEM measurements. The microstructure of the sample was investigated using multibeam bright field imaging and [11 2 0] and [0002] weak-beam dark-field (WBDF) imaging in a FEI Talos F200X TEM operated at 200 keV. A PANalytical MRD diffractometer was used for HRXRD in a triple-axis geometry to determine the composition of the Al_xGa_{1-x}N and estimate the threading dislocation (TD) density of the films. To determine the composition of the Al_xGa_{1-x}N films, scans of symmetric and six asymmetric sets of lattice planes were performed in the 2θ - ω mode and the peak positions were fitted with the Nelson-Riley function to minimize experimental errors.²⁶ The algorithm given by Paduano et al. was then used to determine the film composition.²⁷ Screw and edge TD densities were estimated from the full width at half maximum (FWHM) of ω -scans on AlGaN (0002) and $(10\overline{1}0)$, respectively, using an empirical model developed by Srikant et al. (see supplementary material).²⁸ To probe the stress/strain state and crystalline quality of the undoped and doped Al_{0.30}Ga_{0.70}N films, micro-Raman spectroscopy was performed using a Horiba LabRAM

HR Evolution spectrometer with a $532\,\mathrm{nm}$ laser excitation source. The details of the experimental setup can be found in the supplementary material. Room temperature (RT) Hall measurements were used to measure the carrier density, mobility, and resistivity of the n-type $\mathrm{Al_x}\mathrm{Ga_1}$ xN layers. Atomic force microscopy (AFM) was performed to investigate the surface morphology and roughness of the Ge doped films.

The stress-thickness $(\sigma_f h_f)$ versus thickness (h_f) curves measured during growth are plotted for comparison in Fig. 1 for three samples: undoped Al_{0.30}Ga_{0.70}N, Ge doped Al_{0.30}Ga_{0.70}N $[n \sim 1.6 \quad 10^{19} \text{ cm}^{-3}]$, and Si doped $Al_{0.30}Ga_{0.70}N$ [n $\sim 8.8 ext{ } 10^{18} \text{ cm}^{-3}$]. In the stressthickness versus thickness plot, the slope of the curve at a given thickness represents the incremental stress in the film (σ_f) which is a measure of the stress state at the surface of the growing film, with tensile and compressive stresses denoted by positive and negative values, respectively. In all samples, the negative slope of the stress-thickness versus thickness curves during the AlN buffer layer growth segment indicates an initial compressive incremental stress (2.1 GPa), which arises due to the lattice mismatch between AlN and SiC. The incremental stress decreases slightly near the end of the AlN growth (0.5 GPa), which indicates partial stress relaxation. In all samples, the undoped Al_{0.30}Ga_{0.70}N layer initiates growth in compression (1.8 GPa) and begins to relax with the increasing thickness as shown by the change in the slope of the stress-thickness versus thickness curve. The oscillations in the stress-thickness versus thickness data shown in Fig. 1 arise from beam-steering effects due to slight thickness nonuniformities across the measurement area of the sample.²⁹ For the undoped sample, the incremental compressive stress continues to decrease and transitions into a slight tensile stress (\sim 0.2 GPa) after an \sim 0.6 μ m film thickness. Residual tensile stress has previously been reported in undoped AlGaN grown on SiC³⁰ and undoped GaN grown on Si.³¹ According to the kinetic model of Raghavan et al.,31 this residual tensile stress is associated with the

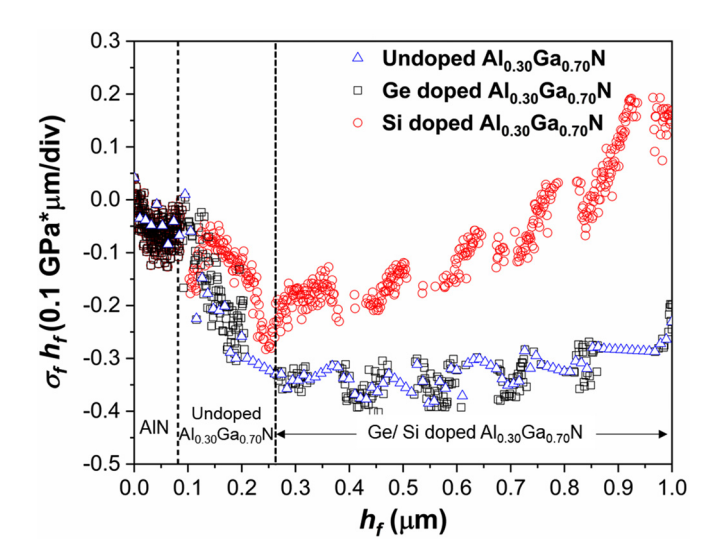


FIG. 1. Stress-thickness vs thickness plot obtained during growth of undoped Al $_{0.30}$ Ga $_{0.70}$ N layer (triangles), with GeH $_4$ addition [n = 1.6 10^{19} /cm 3] (squares) and SiH $_4$ addition [n = 8.8 10^{18} /cm 3] (circles) after \sim 200 nm of layer growth. A transition to tensile stress is measured shortly after SiH $_4$ addition but the film stress is not altered by the addition of GeH $_4$.

undersaturation of adatoms near the dislocation core which is dependent on growth conditions.

When doping the $Al_xGa_{1-x}N$ films with Si, the slope becomes positive soon after SiH_4 is introduced ($\sim 0.2~\mu m$) indicating a transition to a tensile growth stress ($\sim 0.8~GPa$) similar to that previously reported for Si doped $Al_xGa_{1-x}N$ using *in situ* measurements. ^{10,32} In case of Ge-doping, however, the slope remains similar to that of the undoped $Al_{0.30}Ga_{0.70}N$ layer indicating that the addition of Ge during growth does not induce a tensile growth stress in the film. AFM micrographs of the surface morphology of undoped and Ge doped $Al_{0.30}Ga_{0.70}N$ films (Fig. S5) indicate no evident change in surface roughness as a result of Ge doping (R_q of undoped $Al_{0.30}Ga_{0.70}N$: 0.332 nm, R_q of Ge doped $Al_{0.30}Ga_{0.70}N$: 0.372 nm).

Raman spectroscopy and HRXRD measurements were carried out postgrowth to determine the film strain for comparison with the results obtained from the in situ measurements. Typically for Raman measurements of Al_xGa_{1-x}N, the E₂ (high) and A₁ (LO) Raman-active phonon modes can be monitored for residual stress/ strain and thin film crystalline quality assessment.³³ However, since these Al_{0,30}Ga_{0,70}N samples were grown on 6H-SiC substrates, the Al_{0.30}Ga_{0.70}N A₁ (LO) peak is not distinguishable since this portion of the Raman spectra (\sim 750–800 cm $^{-1}$) is dominated by the E₂ (ZO) and E1 (TO) signal intensities of the significantly thicker 6H-SiC substrate. Therefore, the E₂ (high) phonon mode was monitored to determine the effect of Ge and Si doping on the Al_{0.30}Ga_{0.70}N film stress. Representative Raman spectra of all samples are shown in Fig. 2(a). The Si doped Al_{0.30}Ga_{0.70}N film demonstrates a smaller Raman shift relative to the Ge doped and undoped Al_{0.30}Ga_{0.70}N samples, indicative of biaxial tensile stress in the c-plane of the Si doped $Al_{0.30}Ga_{0.70}N$ film (method in the supplementary material).³³ To monitor local variations in the Al_{0.30}Ga_{0.70}N films and to obtain a reasonable sample size, 100 measurements were performed at the center of each Al_{0.30}Ga_{0.70}N sample in an equidistantly spaced two-dimensional map with a sampling area of 100 μ m [Fig. S2]. The peak position of the E2 (high) Al_{0.30}Ga_{0.70}N phonon mode obtained from Raman mapping of the undoped, Ge doped, and Si doped Al_{0.30}Ga_{0.70}N is shown in Fig. 2(b).

As seen in Fig. 2(b), the peak position of the E_2 (high) phonon mode for the undoped, Ge doped, and Si doped $Al_{0.30}Ga_{0.70}N$ follows

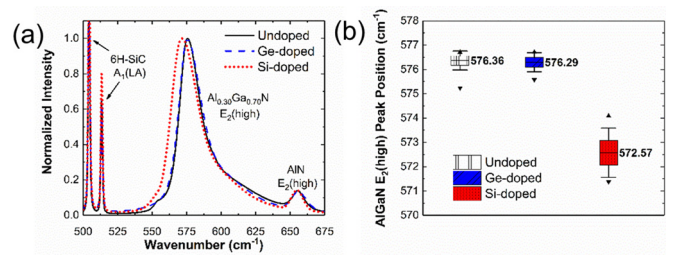


FIG. 2. (a) Representative Raman spectra of the undoped, Ge doped, and Si doped $A_{0.30}Ga_{0.70}N$. Box-and-whisker plots summarize the Raman mapping results for the E_2 (high) (b) peak position. The solid horizontal bar inside the middle of the box represents the mean (mean value labeled), the ends of the box represent a 68% confidence interval, the whiskers represent a 95% confidence interval, and the regular and inverted solid triangles represent the maximum and minimum, respectively. Figure S2 in the supplementary material displays Raman mapping of the E_2 (high) peak position of the Ge doped $Al_{0.30}Ga_{0.70}N$ film (same scale).

the trend observed in Fig. 2(a). There is good agreement between the E_2 (high) peak positions of the undoped and Ge doped $Al_{0.30}Ga_{0.70}N$, suggesting minimal change of the biaxial stress state in the film. In stark contrast, there is a significantly smaller Raman shift for the Si doped $Al_{0.30}Ga_{0.70}N$ which indicates that the film is subjected to a much greater tensile biaxial stress with respect to the undoped and Ge doped films.

The in-plane strain of the Ge doped and Si doped Al_{0.30}Ga_{0.70}N films relative to the undoped Al_{0.30}Ga_{0.70}N film calculated from both Raman and HRXRD measurements is shown in Table I (details of the calculation can be found in the supplementary material). The results from both Raman and HRXRD measurements show that the relative biaxial tensile strain of the Si doped film is much greater than that of the Ge doped film. Normalizing with respect to the Si doped Al_{0.30}Ga_{0.70}N, strain reveals strong agreement between the relative effects of Ge doping and Si doping on Al_{0.30}Ga_{0.70}N films determined from different experimental techniques. The differences in the absolute values of strain measured by the two techniques could be due to the difference in the sampling depth of the two techniques along with the uncertainties in the values of the parameters used to calculate the strain. HRXRD measurements of the undoped, Si doped, and Ge doped Al_{0.30}Ga_{0.70}N samples including 2θ - ω scans and TD densities are reported in Fig. S1 and Table S1, respectively.

To investigate this further, cross-sectional samples were prepared for TEM analysis of the dislocation microstructure of the undoped and Ge doped Al_{0.30}Ga_{0.70}N samples. TEM images of Si doped Al_{0.39}Ga_{0.61}N from a prior study¹⁰ that had a similar doping level are included in the supplementary material (Fig. S4) for comparison. Cross-sectional multibeam bright field TEM images are also included in the supplementary material (Fig. S3). Cross-sectional weak beam dark field (WBDF) TEM images (Fig. 3) were collected at the $\langle 10\overline{1}0 \rangle$ zone axis, tilted toward $g = \langle 0002 \rangle$ and $g = \langle 11\overline{2}0 \rangle$ to examine the behavior of edge and screw type TDs, respectively. Figures 3(a) and 3(b) show the dark field $g = \langle 0002 \rangle$ and $g = \langle 11\overline{2}0 \rangle$ of the undoped Al_{0.30}Ga_{0.70}N, respectively, and Figs. 3(c) and 3(d) show the dark field $g = \langle 0002 \rangle$ and $g = \langle 11\overline{2}0 \rangle$ of the Ge doped $Al_{0.30}Ga_{0.70}N$, respectively. The dashed line across the image in (c) and (d) shows the point where GeH₄ was added during growth. No apparent change in the inclination angle was observed as the dopant was incorporated to a thickness up to $\sim 1 \mu m$. The inclination angle was measured to be 6.9 \pm 4.4 and 7.5 \pm 5.8 for undoped and Ge doped Al_{0.30}Ga_{0.70}N samples, respectively. This is in contrast to studies reported previously that demonstrated a significant change in the dislocation inclination

TABLE I. In-plane strain of Ge doped and Si doped $Al_{0.30}Ga_{0.70}N$ relative to undoped $Al_{0.30}Ga_{0.70}N$ as calculated by Raman and HRXRD measurements. The results have also been normalized (norm.) by the in-plane strain of Si doped $Al_{0.30}Ga_{0.70}N$ calculated from each technique.

	$\varepsilon_{ m a,\ Raman}$				$\varepsilon_{ m a,\ XRD}$		
Ge doped Si doped		10 - 110	10 ⁵ 10 ⁴	2.1	$10^{-4} \pm 1.9$ $10^{-3} \pm 2.2$		
Ge doped (norm.)	2.0	0.018	10	7.4	0.022	10	
Si doped (norm.)		1			1		

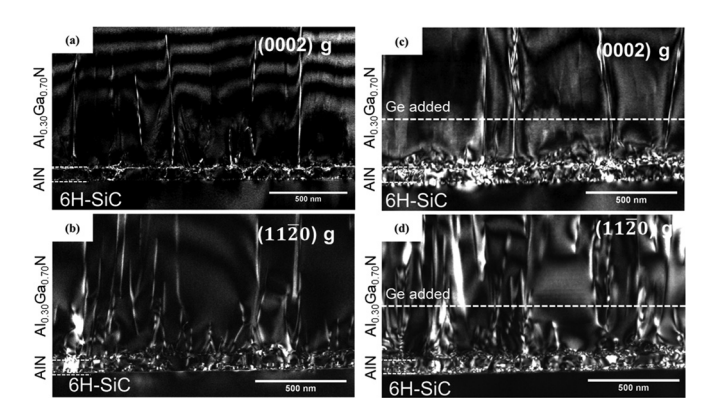


FIG. 3. XTEM weak-beam dark-field TEM images of the undoped Al_{0.30}Ga_{0.70}N (a) $g=\langle 0002\rangle$ and (b) $g=\langle 11\overline{2}0\rangle$ and Ge doped Al_{0.30}Ga_{0.70}N (c) $g=\langle 0002\rangle$ and (d) $g=\langle 11\overline{2}0\rangle$. The dashed lines in (c) and (d) mark the point where GeH₄ was added during growth.

angle for a similar Si doping level in $Al_{0.39}Ga_{0.61}N$ where inclination angles of 9.4 \pm 6.6 and 19.6 \pm 5.7 were reported for undoped and Si doped samples, respectively (see supplementary material, Fig. S4). ¹⁰

In earlier studies, Ge was found to be a shallow donor in GaN.⁴ Therefore, additional studies were performed to measure the room temperature carrier density, resistivity, and mobility in the Ge doped $Al_xGa_{1-x}N$ as a function of Al fraction (Table II). For low Al fraction $Al_xGa_{1-x}N$ (x < 0.5), the resistivity and carrier density did not change significantly with increasing Al fraction. However, it was found that at x = 0.51, the resistivity of the $Al_{0.51}Ga_{0.49}N$ layers increased by a factor of \sim 40, and at x = 0.62, the resistivity was too high to measure accurately, similar to the results reported by Blasco *et al.* for Ge doped $Al_xGa_{1-x}N$ grown by molecular beam epitaxy.¹⁹ The increase in resistivity at high Al fractions may be due to several factors including an increase in donor activation as suggested by Blasco *et al.*¹⁹ and/or the formation of DX centers as predicted by Gordon *et al.*⁴ However, further investigation is needed to conclusively identify the origin of the resistivity changes.

In summary, we have investigated the impacts of Ge doping on film stress and conductivity in ${\rm Al_xGa_{1-x}N}$ with the Al content varying from 0–0.62. Unlike Si doping in ${\rm Al_xGa_{1-x}N}$ films, Ge doping does not induce significant inclination of edge-type TDs or additional tensile stress into the ${\rm Al_xGa_{1-x}N}$ films for low Al fractions (x < 0.5) which is advantageous to reduce the formation of channeling cracks in device structures that include thicker, heavily n-type doped layers. Furthermore, the results of this study suggest that surface-mediated

TABLE II. Resistivity, mobility, and carrier density of Ge doped $Al_xGa_{1-x}N$ layers as determined by Hall-effect measurements at 295 K.

Composition	Resistivity $(10^{-3} \Omega \text{ cm})$	Mobility (cm ² /V s)	Carrier density (10 ¹⁹ cm ³)
Ge: GaN	3	75	4.0
Ge: Al _{0.30} Ga _{0.70} N	7	61	1.6
Ge: Al _{0.41} Ga _{0.59} N	9	43	1.6
Ge: $Al_{0.51}Ga_{0.49}N$	125	20	0.3

climb which propagates inclined TDs in Si doped $Al_xGa_{1-x}N$ is not solely dependent on the Fermi level but is also influenced by the specific chemistry of the dopant species. For example, the greater stability of Si-N compared to Ge-N³⁴ may lead to differences in the chemical potential of the growth surface and the concentration of vacancies near the dislocation core leading to greater tensile stress in the case of Si doping compared to Ge doping.³⁴ Therefore, Ge is a good alternative dopant for low Al fraction $Al_xGa_{1-x}N$ (x < 0.5). For higher Al fractions, further studies are needed to identify the origin of the decrease in Ge doping efficiency.

See supplementary material for related characterization including HRXRD, Raman Spectroscopy, TEM, and AFM.

The authors acknowledge the financial support of the National Science Foundation under Grant Nos. DMR-1410765 and DMR-1808900. This work was also supported by the AFOSR Young Investigator Program (Grant No. FA9550-17-1-0141, Program Officers: Dr. Michael Kendra and Dr. Brett Pokines, also monitored by Dr. Kenneth Goretta). The authors would also like to thank Dr. Mikhail Chubarov for assistance with AFM measurements and critical reading of the manuscript. The authors would also like to thank Dr. Tanushree Choudhury for helpful discussions during the preparation of the manuscript.

REFERENCES

- ¹L. T. Romano, C. G. de Walle, J. W. Ager, W. Götz, and R. S. Kern, J. Appl. Phys. **87**, 7745 (2000).
- ²J. Xie, S. Mita, A. Rice, J. Tweedie, L. Hussey, R. Collazo, and Z. Sitar, Appl. Phys. Lett. 98, 202101 (2011).
- ³R. Kirste, M. P. Hoffmann, E. Sachet, M. Bobea, Z. Bryan, I. Bryan, C. Nenstiel, A. Hoffmann, J.-P. Maria, R. Collazo, and Z. Sitar, Appl. Phys. Lett. 103, 242107 (2013).
- ⁴L. Gordon, J. L. Lyons, A. Janotti, and C. G. de Walle, Phys. Rev. B **89**, 85204 (2014).
- ⁵C. Nenstiel, M. Bügler, G. Callsen, F. Nippert, T. Kure, S. Fritze, A. Dadgar, H. Witte, J. Bläsing, A. Krost, and A. Hoffmann, Phys. Status Solidi-RRL 9, 716 (2015).
- ⁶R. Collazo, S. Mita, J. Xie, A. Rice, J. Tweedie, R. Dalmau, and Z. Sitar, Phys. Status Solidi C 8, 2031 (2011).
- 7S. Terao, M. Iwaya, R. Nakamura, S. Kamiyama, H. Amano, and I. Akasaki, Jpn. J. Appl. Phys., Part 2 40, L195 (2001).
- ⁸A. Krost, A. Dadgar, G. Strassburger, and R. Clos, Phys. Status Solidi **200**, 26 (2003)

- ⁹P. Cantu, F. Wu, P. Waltereit, S. Keller, A. E. Romanov, U. K. Mishra, S. P. DenBaars, and J. S. Speck, Appl. Phys. Lett. 83, 674 (2003).
- ¹⁰J. D. Acord, I. C. Manning, X. Weng, D. W. Snyder, and J. M. Redwing, Appl. Phys. Lett. **93**, 111910 (2008).
- ¹¹P. Cantu, S. Keller, U. K. Mishra, and S. P. DenBaars, Appl. Phys. Lett. 82, 3683 (2003).
- ¹²A. E. Romanov, G. E. Beltz, P. Cantu, F. Wu, S. Keller, S. P. DenBaars, and J. S. Speck, Appl. Phys. Lett. 89, 161922 (2006).
- ¹³A. E. Romanov and J. S. Speck, Appl. Phys. Lett. **83**, 2569 (2003).
- ¹⁴D. M. Follstaedt, S. R. Lee, A. A. Allerman, and J. A. Floro, J. Appl. Phys. **105**, 83507 (2009).
- ¹⁵S. Raghavan, Phys. Rev. B **83**, 52102 (2011).
- ¹⁶A. Dadgar, P. Veit, F. Schulze, J. Bläsing, A. Krtschil, H. Witte, A. Diez, T. Hempel, J. Christen, R. Clos, and A. Krost, Thin Solid Films 515, 4356 (2007).
- ¹⁷S. Fritze, A. Dadgar, H. Witte, M. Bügler, A. Rohrbeck, J. Bläsing, A. Hoffmann, and A. Krost, Appl. Phys. Lett. **100**, 122104 (2012).
- ¹⁸J. Xie, S. Mita, L. Hussey, A. Rice, J. Tweedie, J. LeBeau, R. Collazo, and Z. Sitar, Appl. Phys. Lett. **99**, 141916 (2011).
- ¹⁹R. Blasco, A. Ajay, E. Robin, C. Bougerol, K. Lorentz, L. C. Alves, I. Mouton, L. Amichi, A. Grenier, and E. Monroy, J. Phys. D: Appl. Phys. 52, 125101 (2019).
- ²⁰J. D. Acord, S. Raghavan, D. W. Snyder, and J. M. Redwing, J. Cryst. Growth 272, 65 (2004).
- ²¹S. Raghavan and J. M. Redwing, J. Cryst. Growth 261, 294 (2004).
- ²²S. Raghavan, X. Weng, E. Dickey, and J. M. Redwing, Appl. Phys. Lett. 88, 41904 (2006).
- ²³B. S. Meyerson and J. M. Jasinski, J. Appl. Phys. **61**, 785 (1987).
- ²⁴H. Simka, M. Hierlemann, M. Utz, and K. F. Jensen, J. Electrochem. Soc. 143, 2646 (1996).
- ²⁵Z. Y. Al Balushi and J. M. Redwing, J. Mater. Res. **30**, 2900 (2015).
- ²⁶M. Hermann, F. Furtmayr, F. M. Morales, O. Ambacher, M. Stutzmann, and M. Eickhoff, J. Appl. Phys. **100**, 113531 (2006).
- ²⁷Q. Paduano, D. Weyburne, and S.-Q. Wang, Phys. Status Solidi 188, 821 (2001).
- ²⁸V. Srikant, J. S. Speck, and D. R. Clarke, J. Appl. Phys. **82**, 4286 (1997).
- ²⁹W. G. Breiland, S. R. Lee, and D. D. Koleske, J. Appl. Phys. **95**, 3453 (2004).
- ³⁰I. C. Manning, X. Weng, J. D. Acord, M. A. Fanton, D. W. Snyder, and J. M. Redwing, J. Appl. Phys. **106**, 23506 (2009).
- ³¹S. Raghavan, I. C. Manning, X. Weng, and J. M. Redwing, J. Cryst. Growth 359, 35 (2012).
- ³²I. C. Manning, X. Weng, M. A. Fanton, D. W. Snyder, and J. M. Redwing, J. Cryst. Growth 312, 1301 (2010).
- 33M. Kuball, Surf. Interface Anal. 31, 987–989 (2001).
- 34A. Dadgar, R. Clos, G. Strassburger, F. Schulze, P. Veit, T. Hempel, J. Bläsing, A. Krtschil, I. Daumiller, M. Kunze, A. Kaluza, A. Modlich, M. Kamp, A. Diez, J. Christen, and A. Krost, in *Advances in Solid State Physics*, edited by B. Kramer (Springer, Berlin, Heidelberg, 2004), pp. 313–325.